PAPER

Excitonic effect in black phosphorus oxides

To cite this article: Longxing Chi et al 2022 2D Mater. 9 015007

View the article online for updates and enhancements.

You may also like

- <u>Carrier and spin dynamics of high-density exciton magnetic polarons in Cd_{e.b}Mn_{e.2}Te T Hirase, H Koyama, M Nagata et al.</u>
- Probing interlayer excitons in a vertical van der Waals p-n junction using a scanning probe microscopy technique Mahfujur Rahaman, Christian Wagner, Ashutosh Mukherjee et al.
- Exciton condensation in quantum wells with defects of macroscopic sizes V I Sugakov

2D Materials



RECEIVED 31 August 2021

REVISED

8 October 2021

ACCEPTED FOR PUBLICATION 21 October 2021

PUBLISHED

11 November 2021

PAPER

Excitonic effect in black phosphorus oxides

Longxing Chi^{1,2}, Ming-Hsien Lee³, Ta-Ya Chu^{1,*} and Ye Tao¹

- Advanced Electronics and Photonics Research Centre, National Research Council Canada, Ottawa, Ontario K1A 0R6, Canada
- ² Department of Materials Science and Engineering, University of Toronto, 184 College Street, Toronto, Ontario M5S 3E4, Canada
- Department of Physics, Tamkang University, Tamsui, New Taipei City 25137, Taiwan (ROC)
- * Author to whom any correspondence should be addressed.

E-mail: ta-ya.chu@nrc-cnrc.gc.ca

Keywords: excitonic effect, exciton binding energy, black phosphorus oxides

Supplementary material for this article is available online

Abstract

Two-dimensional (2D) few-layer black phosphorus (BP) with extraordinary electronic and optical properties is an excellent candidate for optoelectronic applications. However, rapid surface oxidation under ambient environment significantly restricts its practicability. Here, we investigate excitonic effect in few-layer BP oxides via first-principle calculation and effective mass approximation. Influence of layer numbers and degree of oxidation on exciton binding energy (EBE) is discussed in detail for the first time. It is found that EBE in BP oxides decreases exponentially with increasing sample thickness and becomes almost oxygen independent over six layers with values similar to that of pristine BP. Instead, oxidation alters excitation probability of excitons in few-layer BP via a direct/indirect bandgap transition.

1. Introduction

Few-layer black phosphorus (FLBP) has emerged as a promising 2D material in optical and optoelectronic applications due to its excellent electronic and optical properties including layer-dependent bandgap, prominent charge-carrier mobility, high current on/off ratios, tunable intraband optical conductivity, etc [1–3]. On the one hand, BP-based photodetectors, electroluminescent devices, spectrometers, photovoltaics are being continuously investigated and upgraded for better device performance [2–8]. On the other hand, issues of rapid carrier recombination rate and low ambient stability result in optical performance penalty in 2D BP and are waiting to be overcome [9–11].

It is critical to decrypt the excitonic effects that dominate optical response of 2D BP owing to significantly reduced dielectric screening and enhanced quantum confinement in low dimensional systems [12]. Excitons in 2D BP exhibit strong optical anisotropy where absorption spectrum, optical permittivity, polarizability vary significantly along different light polarization directions, which can be ascribed to the anisotropic band structure, exciton states and inherent geometries formed in 2D BP [12–14].

Exciton binding energy (EBE) describes the strength of electron–hole (e-h) interaction within excitons and directly determines the carrier recombination rate thereby playing an important role in BP optoelectronic research [9, 15–17]. It is defined as the energy difference between quasiparticle bandgap and optical bandgap [15]. In 2D BP, EBE decreases exponentially with increasing layer numbers, leading to a high optical conductivity for thin samples [12, 13].

The chemical instability of BP primarily originates from surface oxidation. It has been proven both experimentally and theoretically that oxidation occurs at the top BP layer only, which performs as a passivation layer preventing further O₂ penetration into sublayers [18–21]. Besides, the passivation role of the oxide layer can be further enhanced by introducing a coating layer like octadecyltrichlorosilane [22]. In single layer BP, surface oxidation significantly accelerates exciton-exciton annihilation due to introduction of surface defect sites [17]. Furthermore, with the increasing O₂ coverage, EBE increases drastically up to 3 eV at which recombination almost occurs immediately, leading to optoelectronic performance deterioration [23, 24]. Despite of the above limits, black phosphorus oxides (BPOs) are still an excellent candidate for electronic and optical applications:

L Chi et al

high-transconductance field effect transistors, with long-time air resistivity up to 28 days, and tunable photoluminescence (PL) device, controlled by degree of oxidation, have been achieved on BPOs [22, 25, 26]. However, the influence of surface oxidation on excitonic effect of multilayer BP is still unclear; also, interconnection between EBE and dielectric constant, effective mass has rarely been mentioned. Considering the practicability of FLBP and the self-termination feature of BP oxidation, it is of practical significance to investigate the excitonic effects in few-layer black phosphorus oxides (FLBPOs).

In this work, the excitonic effect in FLBPOs has been investigated via density functional theory (DFT) combined with effective mass approximation (EMA). DFT calculations were carried out using CASTEP for geometric optimization, band structure calculation, density of states (DOS) analysis, optical properties calculation [27]. Generalized gradient approximation (GGA) with exchange-correlation functional of Perdew-Burke-Ernzerhof (PBE) in the norm-conserving pseudopotentials were implemented [28–30]. Heyd–Scuseria–Ernzerhof (HSE06) hybrid functional and ultrasoft pseudopotentials were also used for band structure computation for the purpose of bandgap comparison [31, 32]. EBE was estimated using EMA for anisotropic 2D films with a Hamiltonian of:

$$H = -\frac{\hbar^2}{2\mu_x} \frac{\partial^2}{\partial x^2} - \frac{\hbar^2}{2\mu_y} \frac{\partial^2}{\partial y^2} + V_{\text{eh}}(r)$$
 (1)

where $\mu_{x(y)} = \left(1/m_{x(y)}^e + 1/m_{x(y)}^h\right)^{-1}$ is the exciton effective mass [33–35]. $m_{x(y)}^e$, $m_{x(y)}^h$ represents the effective mass of electron, hole along x(y) direction. The electron–hole (e-h) in-plane interaction $V_{\rm eh}(r)$ is described by the Keldysh equation:

$$V_{eh}(r) = -\frac{e^2}{4(\varepsilon_1 + \varepsilon_2)\varepsilon_0 r_0} \left[H_0\left(\frac{r}{r_0}\right) - Y_0\left(\frac{r}{r_0}\right) \right]$$
 (2)

where ε_1 , ε_2 , ε_0 , r_0 , H_0 , Y_0 correspond to relative dielectric constant of upper layers, relative dielectric constant of bottom layers, vacuum permittivity, screening length, Struve function, Bessel function of the 2nd kind, respectively. EBE is equivalent to the system ground state energy. This approach has been widely applied for 2D system computation in which dielectric constant and exciton effective mass are determinants [13, 36-38]. Calculation details have been provided in supplementary material. Different degree of oxidation and layer numbers have been considered during EBE prediction in this work. It is found that influence of O2 coverage on EBE becomes trivial with increasing layer numbers. In the meanwhile, bandgap types, i.e. direct or indirect, determine excitonic effect in FLBPOs rather than EBE. Our research provides further insight into the optoelectronic characteristics of BPOs.

2. Results and discussion

EBE of pristine BP from single layer to six layers have been calculated as shown in figure 1(a). EBE decreases exponentially with increasing BP layers as:

$$E_b = \frac{A}{B + N^{\alpha}} \tag{3}$$

where N is the number of layers and A, B, α are fitting variables related to effective polarizability of 2D layers [13, 39]. This is consistent with previous experimental and theoretical results [13, 16, 36, 39, 40]. Experimental values measured from PL spectrum vary from 0.9 eV to 0.3 eV for single layer BP due to different substrate screening effect [13, 16, 40]. There are also discrepancies in theoretical values, which might be attributed to substrate screening as well as different choices of exchangecorrelation functionals (E_{xc}) [13, 36, 39]. As can be found in figure 1(b), E_{xc} prominently influences DFTcalculated bandgaps that differ to experimental values as well [13, 41-44]. Since EBE is equivalent to energy difference between quasiparticle bandgap and optical bandgap, huge electronic bandgaps usually lead to huge EBE [15]. In the EMA used here, however, EBE calculation involves effective mass instead of electrical bandgap as can be seen from equation (1). Considering the trivial difference in effective mass calculated using both functionals, as shown in table S2 (available online at stacks.iop.org/2DM/9/015007/ mmedia), PBE functional is used for EBE calculation in this work. Despite of difference in EBE magnitudes, our results locate in a reasonable range. Moreover, the predicted layer dependent trend is identical to the one in previous literature.

EBE of FLBPOs with regard to layer numbers at different degree of oxidation is shown in figure 2(b) where corresponding crystal structures of single layer BPOs are exhibited in figure 2(a). Unit cells used for DFT computation are labelled in each structure. Only top BP layer is oxidized in the structural models, in consistent with previous experimental observations [18–20, 22]. The bottom BP layer remains intact considering the bottom layer would be protected against air exposure by substrates in practical cases. Construction of oxide structures are detailed in supplementary material. Exponential decay trend described in equation (3) for pristine BP reappears in its oxides, accompanied by bandgap shrink as shown in figure S3. Fitting curves are represented by dashed lines. At low degree of oxidation (1.66%, black squares), EBE is close to that of pristine BP (grey rhombuses). A highest EBE of 0.69 eV is found in single layer, which is 0.15 eV higher than that of pristine BP (0.54 eV). With the increase of layer numbers up to six, EBE drops down to 0.25 eV equivalent to that of pristine BP. In comparison, at high degree of oxidation (20% \sim 80%), EBE significantly deviates from

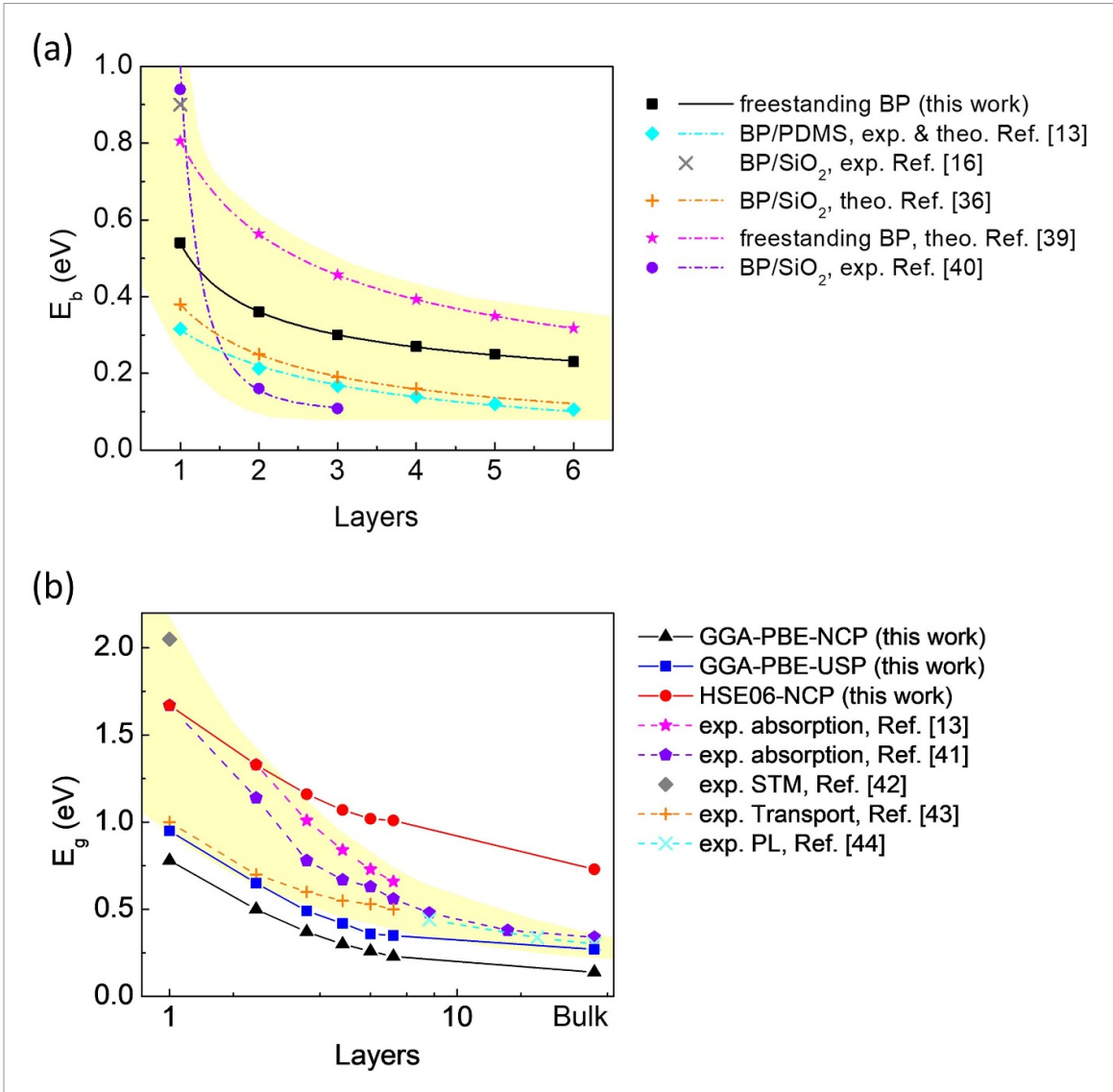


Figure 1. (a) Layer dependence of EBE for pristine BP. Solid lines are our calculations while dashed lines are either experimental (exp) or theoretical (theo) data from previous literature [13, 16, 36, 39, 40]. The yellow region represents the range of EBE reported in previous literatures. (b) Bandgaps of pristine BP calculated using different E_{xc} and pseudopotentials. Solid lines are our estimations while dashed lines are experimental values (exp) from the literature [13, 41–44]. The yellow region represents the range of experimentally measured bandgap reported in previous literatures.

pristine BP in single layer circumstance. A high EBE of 4.31 eV is observed in single layer P₄O₈ (80% oxidation), suggesting a strong electron-hole (e-h)interaction in excitons, giving rise to instant exciton recombination and short exciton radiative lifetime in the system, unfavourable for optoelectronic use [45]. Nevertheless, introducing extra BP layers drastically reduces EBE by an order of magnitude. When there are six layers in total, EBE in BPOs becomes slightly larger than that in pristine BP, suggesting similar exciton radiative lifetime between them. Besides, EBE at different O₂ coverages exhibits the sharpest decrease from single layer to double layers, indicating that the 2nd layer introduces a qualitative change. It is worth mentioning that there are multiple BPO configurations as previously reported [18, 19, 23]. EBE calculated on another P₄O_{0.17} structure also satisfies the exponential decay trend as can be found in the

supplementary material. Another common concern is the influence of water vapours. It has been demonstrated that H₂O will first facilitate surface oxidation on BP then react with BPOs to form phosphoric acid [46]. The 1st step plays a critical role while the 2nd step can be perfectly inhibited via a capping layer [22, 25]. Therefore, from the perspective of practical use, influence of H₂O on BP only involves acceleration in surface oxidation rather than introduction of new functional groups.

To better understand EBE dependence on degree of oxidation, EBE has been replotted with regard to O_2 coverages as exhibited in figure 2(c). The inset is a zoom-in image of the rectangular region corresponding to low O_2 coverages. For single layer (1ML) BPOs, an increasing tendency in EBE can be observed with increasing degree of oxidation, in agreement with previous literature (orange cross, pink cross and

IOP Publishing 2D Mater. 9 (2022) 015007 L Chi et al

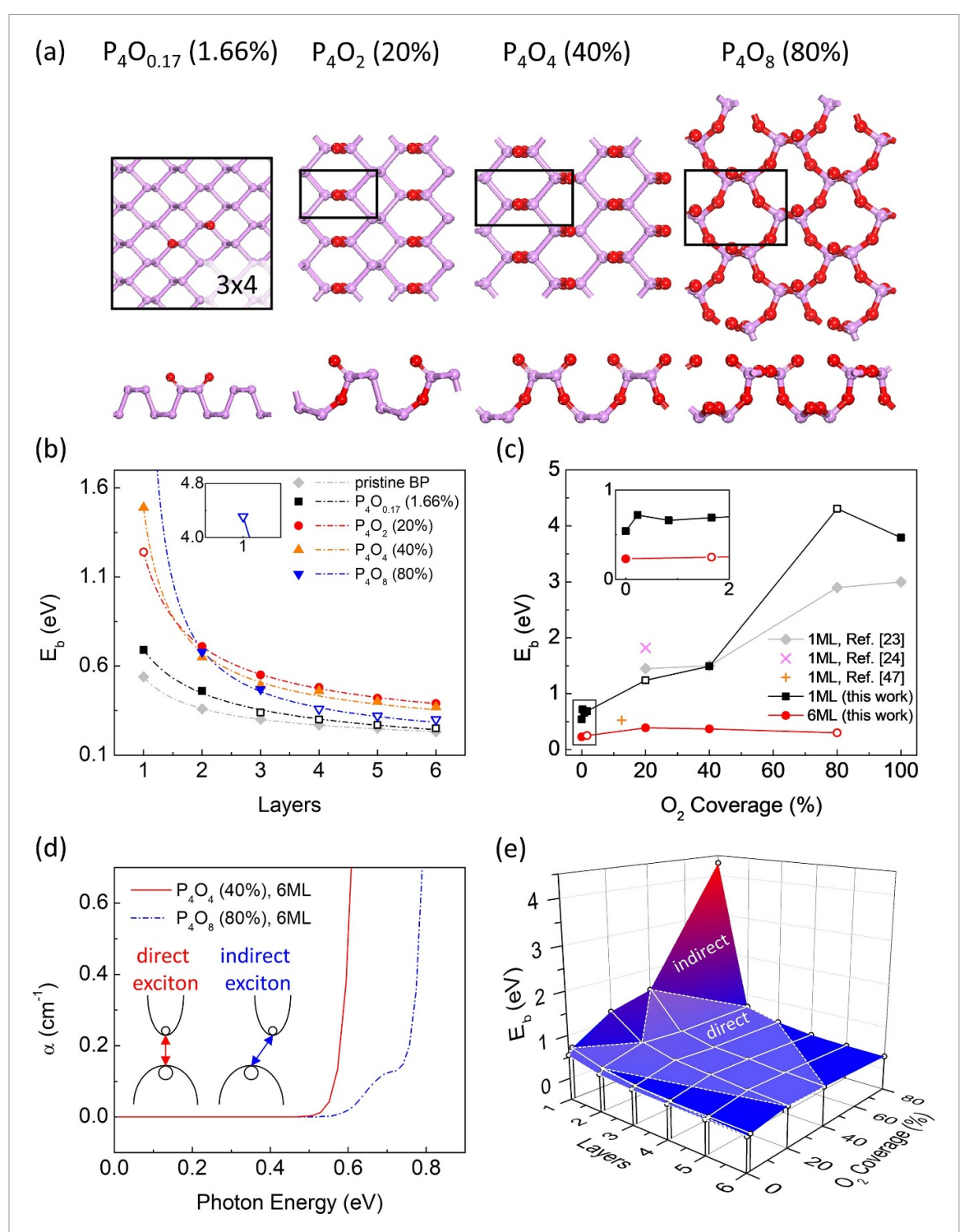


Figure 2. (a) Crystal structure of single layer BPOs. (b) Layer dependence of EBE at different O_2 coverages. Inset is EBE of single layer P_4O_8 . (c) O_2 coverage dependence of EBE at one layer and six layers. Inset is a zoom-in image of squared region. Gray rhombus, pink cross and orange cross are literature values [23, 24, 47] (ML means monolayer). (d) DFT-calculated absorption coefficient of six layers P_4O_4 and P_4O_8 as a function of photon energy. Inset is an illustration of direct/indirect excitons. (e) 3D map of EBE with regard to O_2 coverages and layer numbers. In (b) and (c), open and closed circles correspond to indirect and direct bandgaps, respectively.

grey rhombuses in the graph) [23, 24, 47]. Again, discrepancy in absolute EBE values between literature data and ours can be attributed to different $E_{\rm xc}$ choices, nevertheless overall trend in changes of EBE is identical. For six-layer (6ML) BPOs at different O₂ coverages, EBE is calculated to be 0.46 eV (1.66%), 0.51 eV (20%), 0.53 eV (40%), 0.53 eV

(80%), respectively, comparable to that of pristine BP and no longer exhibits oxygen dependence.

In addition to changes in EBE magnitudes, excitation probability also plays a critical role in excitonic effect in FLBPOs. Two exciton types dominate the absorption probability as illustrated in figure 2(d). Direct excitons are excited by direct

2D Mater. **9** (2022) 015007 L Chi et al

transition without momentum loss while indirect excitons involve indirect transition accompanied with momentum change via phonon absorption or emission. Corresponding excitation probability is proportional to absorption coefficient (α) [48]. Therefore, DFT-calculated absorption coefficient is plotted in figure 2(d) as a function of photon energy. Sixlayer P₄O₄ and P₄O₈ are selected for plotting because both structures have a bandgap of 0.53 eV with the former one direct whereas the latter indirect. It is obvious that absorption coefficient, therefore excitation probability, in direct bandgap system is much higher than indirect system. Exciton types are labelled in figures 2(b) and (c), with solid and hollow symbols representing direct and indirect excitons, respectively. For a better visualization, 3D surface map of EBE with regard to layer numbers and O₂ coverages is plotted in figure 2(e) where direct bandgap region is marked individually. The 3D map further corroborates EBE independence on O2 coverages at high layer numbers. A continuous direct bandgap area exists at O2 coverages between 20% and 40%. Outside the region excitonic effect impairs due to low excitation probability. Indirect bandgaps appear randomly among different wave numbers irrelevant to O₂ coverages as can be seen from figure S4. There is no layer dependence in bandgap type as well: indirect bandgaps occur or eliminate either at single layer or at multilayers. However, based on PDOS shown in figure S5, global bandgaps in FLBPOs, either direct or indirect, are commonly contributed from sublayer P-P bonds instead of P-O or P=O bonds on the oxide layer. It is worth mentioning that bandgap types might be altered by substrates. Overall, excitonic effect in multilayer BPOs is less sensitive to EBE whereas more dominated by O-induced bandgap transitions.

Determinants of EBE, i.e. 2D dielectric constant and exciton effective mass, are discussed in the following paragraphs. Figure 3(a) shows EBE as a function of those two factors. It can be easily found that EBE is negatively related to dielectric constant (black solid line) yet positively related to effective mass (red dashed line). More importantly, EBE is more sensitive to dielectric constant than to effective mass. The value shrinks by an order of magnitude with the change of dielectric constant (vertical scale on the left), while mildly increases as effective mass grows (vertical scale on the right). Layer dependence of dielectric constant is plotted in figure 3(b) in reciprocal scale while the normal scale image is shown in the inset. A linear dependence can be observed through the image for all O2 coverages. Relative dielectric constant (ε_r) is related to polarizability (*P*) by:

$$\frac{1}{\varepsilon_{\rm r}} = 1 - \frac{P}{\varepsilon_0 V_{\rm cell}} \tag{4}$$

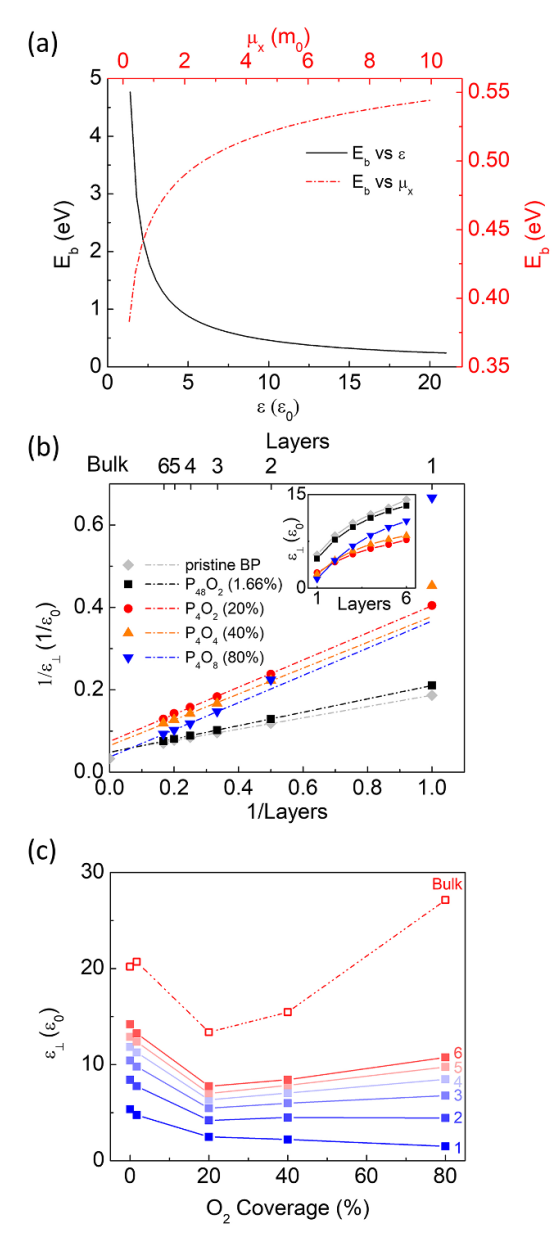


Figure 3. (a) EBE versus dielectric constant and effective mass. (b) Dielectric constant versus layer number in reciprocal scale. Inset is the same image but in conventional scale. (c) Dielectric constant versus O₂ coverages at different layer numbers.

where V_{cell} is the effective 2D cell volume without vacuum space [49]. In the meanwhile, polarizability is proportional to layer numbers (N) by:

$$P(N) = NV_{\text{bulk}} \frac{\varepsilon_0}{2} \left(1 - \frac{1}{\varepsilon_{\text{bulk}}} \right) + b$$
 (5)

where V_{bulk} , $\varepsilon_{\text{bulk}}$, b correspond to volume of the bulk unit cell with two layers, bulk dielectric constant, constant related to surface polarizability, respectively [49]. V_{cell} can be approximated by:

$$V_{cell} \approx \frac{N}{2} V_{bulk}$$
 (6)

for multilayers. Therefore, equation (4) can be rewritten to a linear function between $1/\varepsilon_r$ and 1/N as:

$$\frac{1}{\varepsilon_{\rm r}} = \frac{1}{\varepsilon_{\rm bulk}} + k \frac{1}{N} \tag{7}$$

where $k = -2b/\varepsilon_0$ is the linear constant for curve fitting. Fitting curves are represented by dashed lines in figure 3(b). According to equation (7), bulk dielectric constant can be estimated from vertical intercepts. Here, bulk structure represents an infinite thick BP covered by a single-layer BPOs. As-predicted bulk dielectric constants are 20.2, 20.7, 13.38, 15.46, 27.13 for pristine BP, P₄O_{0.17}, P₄O₂, P₄O₄, P₄O₈, respectively, as plotted in figure 3(c) by hollow squares. The huge dielectric constants guarantee a relatively small EBE around 0.3 eV in FLBPOs. It should be mentioned that dielectric constant for P₄O₄ and P₄O₈ at single layer deviates from their fitting curves. This is because single layer P₄O₄ or P₄O₈ is much thicker than single layer pristine BP, as can be found from table S1. As a result, equation (6) will underrate effective cell volume (V_{cell}) in single-layer case, leading to abovementioned mismatch. However, such a problem disappears in multilayer cases and as-calculated bulk dielectric constant is still trustworthy. Coverage dependence of dielectric constant is also exhibited in figure 3(c). At low O_2 coverage (1.66%), dielectric constant is close to that of pristine BP. At high O_2 coverage (20% \sim 80%), however, dielectric constant becomes sensitive to degree of oxidation. Larger bulk dielectric constant is achieved for higher O2 coverages.

Layer dependence of exciton effective mass are shown in figures 4(a) and (b) where solid and hollow symbols correspond to direct and indirect excitons, respectively. At single layer, effective mass distributes dispersively in both directions. When reached six layers, however, effective mass almost converges regardless of $\rm O_2$ coverages. Averaged effective mass at six layers is 0.093 \pm 0.023 along armchair edge and 0.63 \pm 0.23 along zigzag edge, as marked in the image, indicating a huge anisotropy. More importantly, those values can be approximated as bulk effective mass considering its convergence feature.

Finally, we estimate EBE of bulk BPOs, e.g. $50 \sim 100$ nm thick films, using EMA with a bulk screening length r_0 of:

$$r_0 = \frac{d\varepsilon_{\text{bulk}}}{\varepsilon_1 + \varepsilon_2} \tag{8}$$

where d, $\varepsilon_{\text{bulk}}$, ε_{1} , ε_{2} correspond to film thickness, bulk dielectric constant, capping layer dielectric constant, substrate dielectric constant, respectively [33]. Substituting equation (8) into equation (S3) in supplementary material enables computation of EBE. Bulk dielectric constant and effective mass are required and has been summarized in above context. Capping layer and substrate are treated as vacuum space. As-calculated EBE is plotted in figure 4(c) as a function of sample thickness (also layer numbers) at different O_2 coverages. Points at six layers are collected from figure 2(b) as a reference. EBE

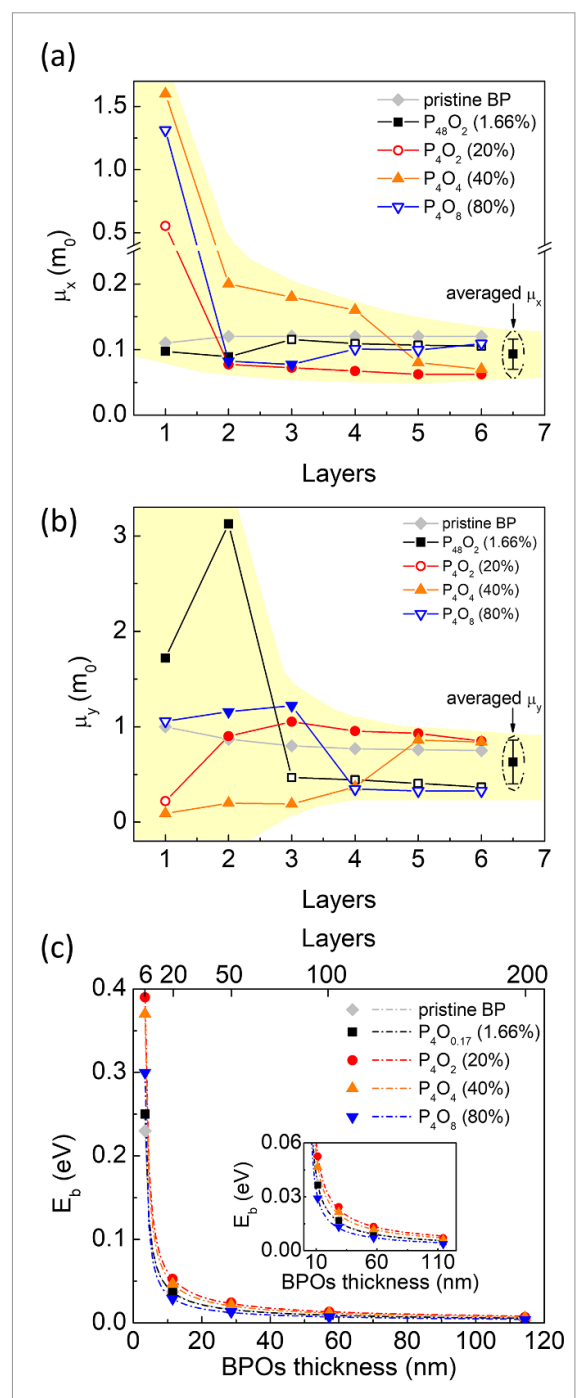


Figure 4. Exciton effective mass as a function of layer numbers along armchair (a) and zigzag (b) edges, respectively. (c) Predicted bulk EBE with regard to sample thickness. Dashed lines are fitting curves. Corresponding layer numbers are shown on the top scale. Inset is a zoom-in image of $E_{\rm b}$ for thick samples. Range of calculated effective mass is yellow highlighted. Open and closed symbols in (a) and (b) correspond to indirect and direct bandgaps, respectively.

in bulk scale (50 \sim 100 nm) converges to few milli electronvolts, which is close to that of free excitons experimentally measured in bulk BP [50]. However, it must be emphasized that EBE itself fails to guarantee excellent optoelectronic performances, bandgap types must take into consideration as abovementioned.

3. Conclusions

In conclusion, we investigated excitonic effect of FLB-POs. It is found that, first, EBE decreases exponentially with regard to layer numbers same as that in pristine BP. Second, EBE in single layer BPOs strongly depends on degree of oxidation. Oversized EBE above 3 eV is achieved at 80% and 100% O2 coverages, indicating large e-h interactions and giving rise to short exciton radiative lifetime. However, EBE in multilayer BPOs converges to pristine BP levels and varies trivially with O2 coverage. Third, different layer numbers and O₂ coverages lead to different excitation probabilities by introducing direct/indirect bandgap transition. As a result, it is the bandgap type rather than EBE that determines excitonic effect in FLB-POs. Fourth, EBE is dominated by dielectric constant and exciton effective mass. The former exhibits linear dependence on layer numbers in reciprocal scale, while the latter converges at high layer numbers regardless of O₂ contents. Finally, EBE in bulk BPOs is estimated with values of few milli electronvolts similar to that of free excitons in bulk pristine BP.

Supplementary material

Calculation details, construction of FLBPO structures, EBE of other BPO configurations, additional figures as mentioned in the text.

Data availability statement

All data that support the findings of this study are included within the article (and any supplementary files).

Acknowledgment

The authors sincerely appreciate research funding provided by National Research Council Canada.

ORCID iDs

Longxing Chi https://orcid.org/0000-0003-4612-

Ming-Hsien Lee https://orcid.org/0000-0003-3956-181X

Ta-Ya Chu b https://orcid.org/0000-0003-2114-

Ye Tao https://orcid.org/0000-0002-0842-6650

References

- Zhang L, Wang B, Zhou Y, Wang C, Chen X and Zhang H 2020 Synthesis techniques, optoelectronic properties, and broadband photodetection of thin-film black phosphorus Adv. Opt. Mater. 8 2000045
- [2] Biswas S, Whitney W S, Grajower M Y, Watanabe K, Taniguchi T, Bechtel H A, Rossman G R and Atwater H A 2021 Tunable intraband optical conductivity and

- polarization-dependent epsilon-near-zero behavior in black phosphorus *Sci. Adv.* 7 eabd4623
- [3] Sui Y, Zhou J, Wang X, Wu L, Zhong S and Li Y 2021 Recent advances in black-phosphorus-based materials for electrochemical energy storage *Mater. Today* 42 117–36
- [4] Yuan S F, Naveh D, Watanabe K, Taniguchi T and Xia F N 2021 A wavelength-scale black phosphorus spectrometer *Nat. Photon.* 15 601–7
- [5] Liu C Y, Guo J S, Yu L W, Li J, Zhang M, Li H, Shi Y C and Dai D X 2021 Silicon/2D-material photodetectors: from near-infrared to mid-infrared *Light Sci. Appl.* 10 21
- [6] Fu Q, Hu Z L, Zhou M F, Lu J P and Ni Z H 2021 Excitonic emission in atomically thin electroluminescent devices Laser Photonics Rev. 15 21
- [7] Chen Y F et al 2021 Unipolar barrier photodetectors based on van der waals heterostructures Nat. Electron. 4 357–63
- [8] Akamatsu T et al 2021 A van der Waals interface that creates in-plane polarization and a spontaneous photovoltaic effect Science 372 68–72
- [9] Wei Y and Long R 2018 Grain boundaries are benign and suppress nonradiative electron–hole recombination in monolayer black phosphorus: a time-domain *ab initio* study *I. Phys. Chem. Lett.* 9 3856–62
- [10] Pei J, Gai X, Yang J, Wang X, Yu Z, Choi D-Y, Luther-Davies B and Lu Y 2016 Producing air-stable monolayers of phosphorene and their defect engineering *Nat. Commun.* 7 10450
- [11] Long R, Fang W and Akimov A V 2016 Nonradiative electron–hole recombination rate is greatly reduced by defects in monolayer black phosphorus: ab initio time domain study J. Phys. Chem. Lett. 7 653–9
- [12] Zhang G W, Huang S Y, Wang F J and Yan H G 2021 Layer-dependent electronic and optical properties of 2D black phosphorus: fundamentals and engineering *Laser Photonics Rev.* 15 2000399
- [13] Zhang G, Chaves A, Huang S, Wang F, Xing Q, Low T and Yan H 2018 Determination of layer-dependent exciton binding energies in few-layer black phosphorus Sci. Adv. 4 eaap9977
- [14] Zhang G, Huang S, Wang F, Xing Q, Song C, Wang C, Lei Y, Huang M and Yan H 2020 The optical conductivity of few-layer black phosphorus by infrared spectroscopy *Nat. Commun.* 11 1847
- [15] Ugeda M M et al 2014 Giant bandgap renormalization and excitonic effects in a monolayer transition metal dichalcogenide semiconductor Nat. Mater. 13 1091–5
- [16] Wang X, Jones A M, Seyler K L, Tran V, Jia Y, Zhao H, Wang H, Yang L, Xu X and Xia F 2015 Highly anisotropic and robust excitons in monolayer black phosphorus *Nat. Nanotechnol.* 10 517–21
- [17] Surrente A, Mitioglu A A, Galkowski K, Klopotowski L, Tabis W, Vignolle B, Maude D K and Plochocka P 2016 Onset of exciton–exciton annihilation in single-layer black phosphorus *Phys. Rev.* B 94 075425
- [18] Ziletti A, Carvalho A, Campbell D K, Coker D F and Castro Neto A H 2015 Oxygen defects in phosphorene *Phys. Rev.* Lett. 114 046801
- [19] Lu J, Wu J, Carvalho A, Ziletti A, Liu H, Tan J, Chen Y, Castro Neto A H, Özyilmaz B and Sow C H 2015 Bandgap engineering of phosphorene by laser oxidation toward functional 2D materials ACS Nano 9 10411–21
- [20] Edmonds M T, Tadich A, Carvalho A, Ziletti A, O'Donnell K M, Koenig S P, Coker D F, Özyilmaz B, Neto A H C and Fuhrer M S 2015 Creating a stable oxide at the surface of black phosphorus ACS Appl. Mater. Interfaces 7 14557–62
- [21] Gómez-Pérez J, Barna B, Tóth I Y, Kónya Z and Kukovecz Á 2018 Quantitative tracking of the oxidation of black phosphorus in the few-layer regime ACS Omega 3 12482–8

- [22] Artel V, Guo Q, Cohen H, Gasper R, Ramasubramaniam A, Xia F and Naveh D 2017 Protective molecular passivation of black phosphorus Npj 2D Mater. Appl. 1 6
- [23] Lu Y and Zhu X 2019 Superbound excitons in 2D phosphorene oxides J. Phys. Chem. A 123 21–25
- [24] Sadki S and Drissi L B 2018 Tunable optical and excitonic properties of phosphorene via oxidation J. Phys.: Condens. Matter 30 255703
- [25] Wood J D, Wells S A, Jariwala D, Chen K-S, Cho E, Sangwan V K, Liu X, Lauhon L J, Marks T J and Hersam M C 2014 Effective passivation of exfoliated black phosphorus transistors against ambient degradation *Nano Lett.* 14 6964–70
- [26] Gan Z X, Sun L L, Wu X L, Meng M, Shen J C and Chu P K 2015 Tunable photoluminescence from sheet-like black phosphorus crystal by electrochemical oxidation Appl. Phys. Lett. 107 021901
- [27] Clark S J, Segall M D, Pickard C J, Hasnip P J, Probert M I J, Refson K and Payne M C 2005 First principles methods using castep Z. Kristallogr. Cryst. Mater. 220 567–70
- [28] Kresse G and Joubert D 1999 From ultrasoft pseudopotentials to the projector augmented-wave method Phys. Rev. B 59 1758–75
- [29] Grimme S 2006 Semiempirical GGA-type density functional constructed with a long-range dispersion correction *J. Comput. Chem.* 27 1787–99
- [30] Payne M C, Teter M P, Allan D C, Arias T A and Joannopoulos J D 1992 Iterative minimization techniques for *ab initio* total-energy calculations: molecular dynamics and conjugate gradients *Rev. Mod. Phys.* 64 1045–97
- [31] Perdew J P, Burke K and Ernzerhof M 1998 Perdew, burke, and ernzerhof reply Phys. Rev. Lett. 80 891
- [32] Heyd J, Scuseria G E and Ernzerhof M 2003 Hybrid functionals based on a screened coulomb potential *J. Chem. Phys.* 118 8207–15
- [33] Keldysh L 1979 Coulomb interaction in thin semiconductor and semimetal films JETP Lett. 29 658
- [34] Prada E, Alvarez J V, Narasimha-Acharya K L, Bailen F J and Palacios J J 2015 Effective-mass theory for the anisotropic exciton in two-dimensional crystals: application to phosphorene *Phys. Rev.* B 91 245421
- [35] Rodin A S, Carvalho A and Castro Neto A H 2014 Excitons in anisotropic two-dimensional semiconducting crystals *Phys. Rev.* B 90 075429
- [36] Castellanos-Gomez A et al 2014 Isolation and characterization of few-layer black phosphorus 2D Mater. 1 025001

- [37] van Tuan D, Yang M and Dery H 2018 Coulomb interaction in monolayer transition-metal dichalcogenides *Phys. Rev.* B 98 125308
- [38] Berkelbach T C, Hybertsen M S and Reichman D R 2013 Theory of neutral and charged excitons in monolayer transition metal dichalcogenides *Phys. Rev.* B 88 045318
- [39] Tran V, Soklaski R, Liang Y and Yang L 2014 Layer-controlled band gap and anisotropic excitons in few-layer black phosphorus *Phys. Rev.* B 89 235319
- [40] Tian R, Fei R, Hu S, Li T, Zheng B, Shi Y, Zhao J, Zhang L, Gan X and Wang X 2020 Observation of excitonic series in monolayer and few-layer black phosphorus *Phys. Rev.* B 101 235407
- [41] Chen C et al 2019 Bright mid-infrared photoluminescence from thin-film black phosphorus Nano Lett. 19 1488–93
- [42] Liang L, Wang J, Lin W, Sumpter B G, Meunier V and Pan M 2014 Electronic bandgap and edge reconstruction in phosphorene materials *Nano Lett.* 14 6400–6
- [43] Zhang G, Huang S, Chaves A, Song C, Özçelik V O, Low T and Yan H 2017 Infrared fingerprints of few-layer black phosphorus Nat. Commun. 8 14071
- [44] Das S, Zhang W, Demarteau M, Hoffmann A, Dubey M and Roelofs A 2014 Tunable transport gap in phosphorene *Nano Lett.* 14 5733–9
- [45] Chen H et al 2019 Nonlinear nanophotonics with 2D transition metal dichalcogenides Comprehensive Nanoscience and Nanotechnology 2nd edn, ed D L Andrews (New York: Academic) 1 305–18
- [46] Favron A, Gaufrès E, Fossard F, Phaneuf-L'Heureux A-L, Tang N Y W, Lévesque P L, Loiseau A, Leonelli R, Francoeur S and Martel R 2015 Photooxidation and quantum confinement effects in exfoliated black phosphorus Nat. Mater. 14 826–32
- [47] Xu W P and Xu H 2018 Role of surface adsorption in tuning the properties of black phosphorus *Phys. Chem. Chem. Phys.* 20 112–7
- [48] Jenkins R and de Vries J L 1970 Excitation Probability Worked Examples in X-Ray Analysis (Berlin: Springer) (https://doi. org/10.1007/978-1-4899-2647-0_34)
- [49] Kumar P, Bhadoria B S, Kumar S, Bhowmick S, Chauhan Y S and Agarwal A 2016 Thickness and electric-field-dependent polarizability and dielectric constant in phosphorene *Phys.* Rev. B 93 195428
- [50] Carré E, Sponza L, Lusson A, Stenger I, Gaufrès E, Loiseau A and Barjon J 2021 Excitons in bulk black phosphorus evidenced by photoluminescence at low temperature 2D Mater. 8 021001